LISA Pathfinder closed-loop analysis: a model breakdown of the in-loop observables

IOP Conf. Series: Journal of Physics: Conf. Series **840** (2017) 012038 doi:10.1088/1742-6596/840/1/012038

LISA Pathfinder closed-loop analysis: a model breakdown of the in-loop observables

LISA Pathfinder collaboration

E-mail: henri.inchauspe@apc.in2p3.fr

Abstract. This paper describes a methodology to analyze, in the frequency domain, the steady-state control performances of the LISA Pathfinder mission. In particular, it provides a technical framework to give a comprehensive understanding of the spectra of all the degrees of freedom by breaking them down into their various physical origins, hence bringing out the major contributions of the control residuals. A reconstruction of the measured in-loop output, extracted from a model of the closed-loop system, is shown as an instance to illustrate the potential of such a model breakdown of the data.

1. Introduction

The LISA Pathfinder mission [3] has been operating since March 2016 and has demonstrated the feasibility of sub-femto-g free-fall of test masses necessary to build a LISA-like gravitational waves observatory in space [2]. While the publication [2] is mostly concerned by acceleration noise performances along the most sensitive x-axis, LISA Pathfinder has shown impressive performances and stability for the other measurement channels. Those extra degrees of freedom, though not the main channel of interest, are of great importance for the satellite's closed-loop control framework, the so-called *Drag-Free and Attitude Control System (DFACS)* [6]. This core subsystem has been designed by *Airbus Defence & Space* to achieve the specific requirements of LISA Pathfinder. To reach such an acceleration sensitivity along x-axis implies a very quiet and stable environment, and in particular, a very stable test-mass position and orientation, along and around all the geometrical axes, in order to avoid coupling to the sensitive x-axis through cross-talks and stiffnesses, for instance.

The left-hand diagram of the figure 1 shows the scheme of the experiment. Two cubic test masses of around 2kg are almost free-floating inside housings whose inside walls have electrodes facing the test masses. These electrodes, forming a set of capacitances with the test mass surface, are solicited for sensing and control of the mass inside its housing. While the test mass positions can be corrected through electrostatic actuation along x_2-axis and θ_2, η, ϕ angles (*suspension control*), the other degrees of freedom x_1, y, z and θ_1 are controlled exclusively through spacecraft micro-propulsion (*drag-free control*). The only exception to that is made for the *attitude control*, for which test masses are actuated along y, z and θ_1, in order to induce a torque command on the spacecraft from drag-free control. The role of the *DFACS* is to maintain the test masses parallel to the electrode surfaces, and centered in their housing, except for test mass 2 along the x-axis which is constrained to maintain null relative displacement w.r.t the test mass 1 (x_{12} coordinate is in-loop instead of x_2).

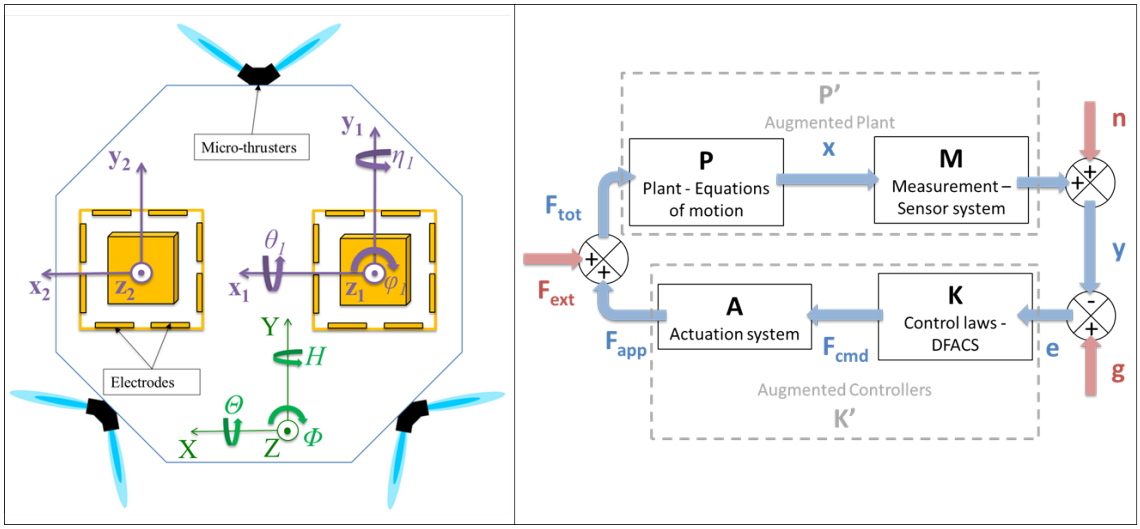

Figure 1: *Left-hand figure*: Simplified sketch of the experiment scheme, representing essentially the system of the three bodies involved and the coordinate systems used to describe the motion of the bodies one w.r.t the others. *Right-hand figure*: Diagram of the closed loop system. The closed loop system is excited in 3 different channels: the guidance signal g, the sensing noise n, and the external forces F_{ext}.

2. Study of LISA Pathfinder closed loop system

2.1. The sensitivity closed-loop transfer functions

The LISA Pathfinder closed loop system, approximated as a linear system in this document, can be fully represented by a set of four (non-independent) closed loop transfer function, often named as "The Gang of Four" in the literature [4], denoting the influence of system inputs coming from system environment (noise, disturbances) over the in-loop controlled variables (measurements, commanded forces, system states...). These transfer functions are all functions of every open-loop transfer functions involved in the closed loop system (Plant, Measurement and Actuation blocks, Controllers etc. see block diagram in figure 1):

- The *sensitivity function* $S(f)$, or *S-gain*, denotes the sensitivity of the in-loop sensors outputs $\vec{o}$ to the sensing noise $\vec{n}$ of all the sensors. $S(f)$ is a 15x15 matrix of transfer functions in LISA Pathfinder's case.

- The *load disturbance sensitivity function* $L(f)$, or the *L-gain*, calls for the sensitivity of the state variable $\vec{x}$ (displacements for the dynamical states) to the direct force and torque noises $\vec{F}_{ext}$ applied on the test masses (along every degree of freedom). $L(f)$ is a 15x18 matrix of transfer functions.

- The *complementary sensitivity function* $T(f)$, or the *T-gain*, stands for the sensitivity of the state variable $\vec{x}$ to the sensing noise $\vec{n}$ of all the sensors.. $T(f)$ is a 15x15 matrix of transfer functions.

The fourth and last one is not be used in the present analysis. The relationships between these closed loop functions and the sub-blocks in figure 1 are given by equations 1:

$$S(f) = \frac{1}{1+P'K'} \qquad L(f) = \frac{P'}{1+P'K'}$$
$$T(f) = \frac{P'K'}{1+P'K'} \tag{1}$$

where it can be seen that the functions are not independent (for instance, S and T are constrained by the identity $S+T=1$).

From this definition, it follows that measuring this set of transfer functions allows to fully characterize the closed loop behavior of the linear system. Conversely, having a sufficiently reliable model of these characteristic functions allows one to predict the spectral behavior of the (physical) in-loop variables, provided that one has some knowledge of the external disturbing signals exciting the loop. Both those aspects will be considered in the next section.

2.2. In-loop sensing outputs and states breakdowns

The LISA Pathfinder collaboration has implemented a full linear state space modeling of the closed loop system [8], from which the closed loop functions discussed in section 2.1 can be extracted. Hence, an interesting comparison can be performed, using the state space model and a measurement of the external signals to reconstruct an estimate of the in-loop variables. By focusing on the sensing outputs $\vec{Y}$ (equation 2) and state variables $\vec{X}$ (equation 3) , one can express those quantities w.r.t. the external signals in the diagram of the figure 1:

$$\tilde{Y}^q = \sum_{p=x,y,z,\theta,\eta,\phi} L^{qp}_{gain}\tilde{F}^p_{ext} + \sum_{p=x,y,z,\theta,\eta,\phi} S^{qp}_{gain}\tilde{n}^p + \sum_{p=x,y,z,\theta,\eta,\phi} T^{qp}_{gain}\tilde{g}^p \tag{2}$$

$$\tilde{X}^q = \sum_{p=x,y,z,\theta,\eta,\phi} L^{qp}_{gain}\tilde{F}^p_{ext} - \sum_{p=x,y,z,\theta,\eta,\phi} T^{qp}_{gain}\tilde{n}^p + \sum_{p=x,y,z,\theta,\eta,\phi} T^{qp}_{gain}\tilde{g}^p \tag{3}$$

$$\tilde{F}^q_{cmd} = \sum_{p=x,y,z,\theta,\eta,\phi} L^{qp}_{gain}\tilde{F}^p_{ext} - \sum_{p=x,y,z,\theta,\eta,\phi} T^{qp}_{gain}\tilde{n}^p + \sum_{p=x,y,z,\theta,\eta,\phi} T^{qp}_{gain}\tilde{g}^p \tag{4}$$

One notes that the sensing noise does not influence $\vec{Y}$ and $\vec{X}$ in the same manner. Indeed, while the double integrator behavior of the plant makes it respond efficiently at low frequency, the control gain is also important at low frequency, resulting in a very low *S-gain* at low frequency. Hence, one does not see any sensing noise in the low frequency part of $\vec{Y}$ spectrum. However, for the very same reason, the *T-gain* is maximal at very low frequency, thus suggesting a perfect correlation between the state $\vec{X}$ and the noise $\vec{n}$ in that domain. This can be viewed even more clearly in considering that the high control gain in that frequency domain tends to "shake" the test mass in order to cancel the sensing noise, the latter being undistinguishable from real motion from *DFACS*'s point of view.

From equations 2, 3 and 4, one can extract two sorts of information. First, one can identify where the sensing outputs and the commanded forces, both delivered by the telemetry, can reflect the out-of-loop signals, i.e. the sensing and force noises, thus constituting a direct measurement of those. As an example, at sufficiently high frequency the plant gain is so large that any commanded forces applied on the masses will result in no displacement at all, meaning that one directly observes the sensing noise from the sensing output. That property is directly inferable from the value of the S-function at high frequency, which tends towards unity. For the force noise though, one can equally well subtract the calibrated commanded forces to retrieve the external noisy force, thus avoiding control in-loop features.

3. Output decomposition from model: instance of the angle ϕ_1

Once the out-of-loop signals have been measured or estimated, one can reconstruct assessed versions of the outputs. One can also decomposed those quantities w.r.t. the contributions from each individual noise sources. This technic is a very useful tool for diagnose purposes, as will be seen below. In confronting these estimates to the actually observed quantities, one verifies that the behavior of each controlled degree of freedom is well understood. The figure 2 exhibits such a comparison between modeled and measured displacement spectrum, in the case of the ϕ_1 degree of freedom (i.e. Cardan rotation angle around the z_1-axis, cf. figure 1), measured by the interferometer through differential wavefront sensing [7]. In the same plot is drawn the estimated contributions to the spectrum from the various noise sources.

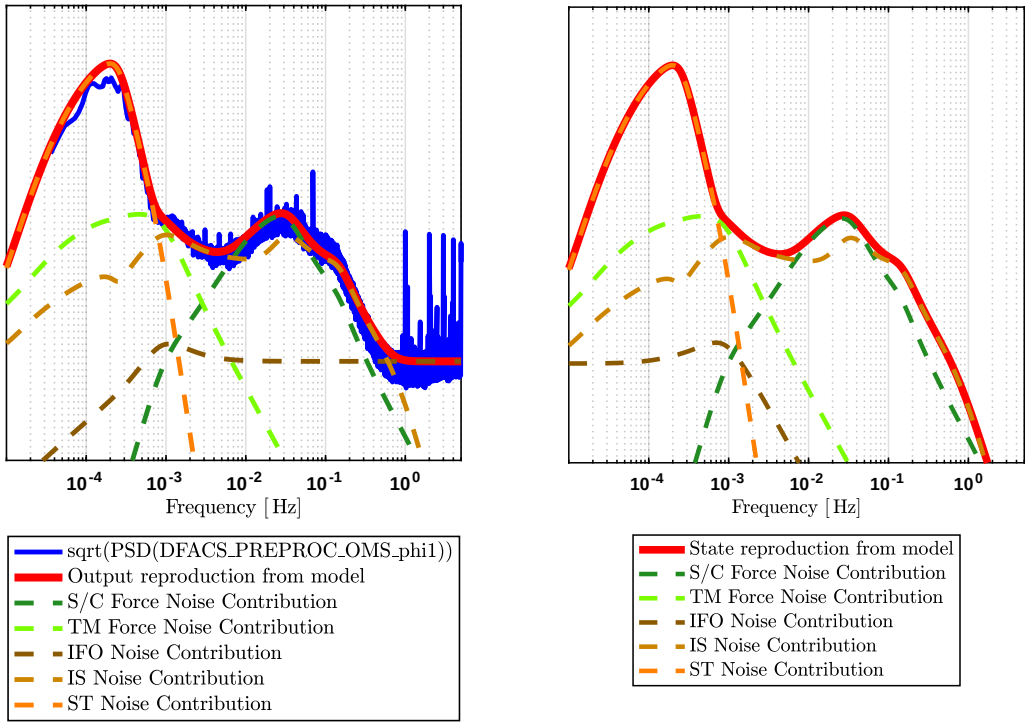

Figure 2: Decomposition in the frequency domain of the measurement outputs (on the left) and the modeled true dynamical states (on the right) into the various contributions from the sensing noise and the external disturbances. The blue curve comes directly from LPF data corresponding to the long noise run (i.e. free of any calibration signal) in nominal science mode of April 2016 (**dataset from 2016-04-04 00:00 UTC to 2016-04-14 00:00 UTC**[1]). The red curve is built from modeled closed loop transfer functions (SSM model) with noise level listed in the table above. Dashed curves give the individual contributions of each of the noise channels. These plots help to identify what are the physical phenomena explaining the output spectrum in the different frequency band.

The case of ϕ angular displacement of the test masses is of particular interest. Indeed, in analyzing what are the major contributing noise sources to ϕ_1 observed displacement in figure 2, one notes that various sources come equally into play, depending on the frequency bandwidth of focus. At very low frequency, a large bump is clearly imputed to the star tracker noise, which indeed, though very indirectly, affects the in-loop test masses angular

[1] The y-scales are voluntarily hidden to keep data exclusivity for an upcoming publication [5]

variables. The attitude control strategy of LISA Pathfinder is such that the spacecraft reacts to star tracker error signals, say around Φ, by first pushing the test masses away one from the other along y_1 and y_2. Then the Drag-Free control immediately sees the induced differential motion between test masses, and commands the spacecraft to rotate in order to compensate that small linear motion. The spacecraft rotation entails in its turn a misalignment between the spacecraft and the test masses reference frame, and finally the suspension control, i.e. the capacitive actuation system, commands torques on the test masses to reorient them inside their housing. Hence, the link between the star tracker signal and the test masses rotation is far from being direct, though obviously large in the figure 2. The level of that contribution is both due to an increase of the star tracker noise and a significantly high authority of the attitude control gain typically below 10^{-3}Hz. In the intermediate frequency band, i.e. between 10^{-2}Hz and 10^{-1}Hz, the Drag-Free control gain decreases significantly and reaches its minimum, thus allowing spacecraft to test masses relative displacements, both linear and angular. In the latter case, it will force the suspension control to correct these noisy rotations. However, because the control gain is also relatively weak in that frequency band, angular displacements are allowed to pass through the loop. At very high frequency finally, the commanded forces become inefficient because of the test masse inertia and one observes the interferometer sensing noise only which provides, as already discussed in section 2.2, a way to measure it.

4. Conclusion

A strategy to analyze *DFACS* performances and interpret control residuals has been developed and is presented in this paper. It allows for a full understanding of the LISA Pathfinder general in-loop dynamics, which has a significant impact on the noise performances along the optical sensitive axis, and more generally, on the future LISA observatory [1]. According to figure 2, the state space model developed by the collaboration is shown to be remarkably reliable in explaining the observed system in-loop behavior, hence giving the state space model a very interesting power of diagnosis. The reliability of the model seems to argue in favor of the assumptions of linearity and stationarity of the system. This capacity of the model to reliably represent LISA Pathfinder's closed loop system is also very interesting in the LISA context, especially for the upcoming task of transferring the knowledge acquired from LISA Pathfinder experiment to LISA simulations and design.

Acknowledgements

E.P. and H.I would like to acknowledge the financial support of the UnivEarthS Labex program at Sorbonne Paris Cité (ANR-10-LABX-0023 and ANR-11-IDEX-0005-02) and the French space agency CNES for its financial support during these studies.

References

[1] Pau Amaro-Seoane et al. "Laser Interferometer Space Antenna". In: *arXiv:1702.00786 [astro-ph]* (Feb. 2017). arXiv: 1702.00786. URL: http://arxiv.org/abs/1702.00786 (visited on 02/16/2017).

[2] M. Armano et al. "Sub-Femto-g Free Fall for Space-Based Gravitational Wave Observatories: LISA Pathfinder Results". In: *Physical Review Letters* 116.23 (June 2016), p. 231101. DOI: 10.1103/PhysRevLett.116.231101. URL: http://link.aps.org/doi/10.1103/PhysRevLett.116.231101 (visited on 10/24/2016).

[3] M. Armano et al. "The LISA Pathfinder Mission". en. In: *Journal of Physics: Conference Series* 610.1 (May 2015), p. 012005. ISSN: 1742-6596. DOI: 10.1088/1742-6596/610/1/012005. URL: http://iopscience.iop.org/1742-6596/610/1/012005 (visited on 06/19/2015).

[4] Karl Johan Åström and Richard M. Murray. *Feedback systems: an introduction for scientists and engineers*. anglais. Princeton, Royaume-Uni de Grande-Bretagne et d'Irlande du Nord, 2008. ISBN: 978-0-691-13576-2.

[5] LISA Pathfinder collaboration. "LISA Pathfinder drag-free performances: frequency domain analysis of the in-loop dynamics". In: *N.D.* (Upcoming publication).

[6] Walter Fichter et al. "LISA Pathfinder drag-free control and system implications". en. In: *Classical and Quantum Gravity* 22.10 (Apr. 2005), S139. ISSN: 0264-9381. DOI: 10.1088/0264-9381/22/10/002. URL: http://iopscience.iop.org/article/10.1088/0264-9381/22/10/002/meta (visited on 02/16/2017).

[7] G. Heinzel et al. "The LTP interferometer and phasemeter". en. In: *Classical and Quantum Gravity* 21.5 (Feb. 2004), S581. ISSN: 0264-9381. DOI: 10.1088/0264-9381/21/5/029. URL: http://iopscience.iop.org/article/10.1088/0264-9381/21/5/029/meta (visited on 02/16/2017).

[8] Mario Weyrich. "Modelling and Analyses of the LISA Pathfinder Technology Experiment". PhD thesis. University of Stuttgart, 2008.